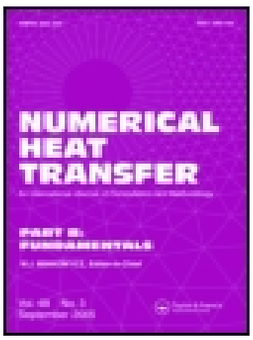

Taylor & Francis
Taylor & Francis Group

Numerical Heat Transfer, Part B: Fundamentals
An International Journal of Computation and Methodology

ISSN: 1040-7790 (Print) 1521-0626 (Online) Journal homepage: https://www.tandfonline.com/loi/unhb20

Coupled level-set and volume-of-fluid method for two-phase flow calculations

Yeng-Yung Tsui, Cheng-Yen Liu & Shi-Wen Lin

To cite this article: Yeng-Yung Tsui, Cheng-Yen Liu & Shi-Wen Lin (2017) Coupled level-set and volume-of-fluid method for two-phase flow calculations, Numerical Heat Transfer, Part B: Fundamentals, 71:2, 173-185, DOI: 10.1080/10407790.2016.1265311

To link to this article: https://doi.org/10.1080/10407790.2016.1265311

Published online: 15 Feb 2017.

NUMERICAL HEAT TRANSFER, PART B
2017, VOL. 71, NO. 2, 173–185
http://dx.doi.org/10.1080/10407790.2016.1265311

Taylor & Francis
Taylor & Francis Group

Coupled level-set and volume-of-fluid method for two-phase flow calculations

Yeng-Yung Tsui, Cheng-Yen Liu, and Shi-Wen Lin

Department of Mechanical Engineering, National Chiao Tung University, Hsinchu, Taiwan, Republic of China

ABSTRACT

In simulating two-phase flows, the volume-of-fluid (VOF) method has the advantage of mass conservation while with the level-set (LS) method, the surface tension force can be calculated more accurately. In this study, we present a coupling method which combines the advantages of both methods. The volume-of-fluid (VOF) method adopted in the calculation is the conservative interpolation scheme for interface tracking method proposed recently by the authors. Based on the location of the interface calculated from the VOF, the LS function is obtained by solving the equation used in the LS method for re-initialization without needing to solve its advection equation. A high-resolution-bounded scheme within the frame of finite-volume methods is used to solve the re-initialization equation. This scheme is verified by considering a variety of interface geometries. A circular bubble at equilibrium is used to assess the coupled LS and VOF method by examining the spurious currents generated in the bubble. Three-dimensional calculations are conducted to study the rising of a bubble in the quiescent water.

ARTICLE HISTORY
Received 12 August 2016
Accepted 4 November 2016

Introduction

The most challenging task in simulating two-phase flows is to treat the interface between the two phases of the fluid. The difficulty comes from the evolvement of this surface boundary, along with the sharp changes in density and viscosity. The most popular approaches used to treat the motion of the interface include the volume of fluid (VOF) and level-set (LS) methods. In LS methods, the level set function represents a signed distance which is positive on one fluid side and negative on the other side [1]. The advection equation for the LS function is of hyperbolic type which can be solved with use of the well-developed methods for high-speed flows, such as the total variation diminishing (TVD) and essentially non-oscillatory (ENO) methods. The position, together with the curvature, of the interface can be calculated accurately due to the smooth characteristics of this function. The major drawback of the method is the lack of mass conservation, because the distance characteristics of the LS function will be lost after solving the advection equation. Therefore, a re-initialization procedure becomes necessary [2–4]. In VOF methods, the VOF function represents the fraction of volume in the grid cell occupied by one of the two fluids [5]. Although it has the same form of advection equation as the LS function, it is rather difficult to be solved accurately due to its sharp change in the transition region of the interface. In the VOF-based piecewise linear interface construction (PLIC) method [6–9], the gradient of the interface is required for reconstruction of the interface from the VOF distribution. Besides, the interface curvature is also required in modeling the surface tension force [10]. These geometric properties cannot be determined accurately from the VOF function. The major advantage of the VOF method over the LS method is that the mass conservation is preserved.

CONTACT Yeng-Yung Tsui yytsui@mail.nctu.edu.tw Department of Mechanical Engineering, National Chiao Tung University, Hsinchu 300, Taiwan, Republic of China.
Color versions of one or more of the figures in this article can be found online on at www.tandfonline.com/unhb.

Nomenclature

d	diameter of bubble
$d(\vec{r})$	distance function
Eo	Eotvos number
$\vec{F}_\sigma$	surface tension force
$\vec{g}$	gravitational acceleration
$H(\phi)$	smoothed Heaviside function
Mo	Morton number
$\vec{n}$	unit normal vector
P	pressure
Re	Reynolds number
$S(\phi^0)$	sign function
$\vec{s}_j$	surface vector for the jth cell face
$\vec{s}_j^{\,w}$	surface vector for the wetted cell face j
$\vec{V}$	velocity vector
$\vec{V}_j$	velocity vector on the jth cell face
α	volume-of-fluid function
$\delta(\phi)$	Dirac delta function
$\vec{\delta}_{U-f}$	distance vector from upstream centroid U to face f
Δh	cell size
Δt	time-step size
Δv	cell volume
ε	numerical interface width
ϕ	level set function
ϕ^o	initial value of the LS
γ	flux limiter
κ	interface curvature
μ	fluid viscosity
ρ	fluid density
σ	surface tension
$\tilde{\tilde{\tau}}$	viscous stress

Subscripts

Ci	ith neighboring cell
f	cell face
g	gas phase
j	jth cell face
l	liquid phase
ni	ith vertex node
P	primary cell

Superscripts

n, $n+1$	time-step numbers
n, o	new and old time steps
w	wetted area of the cell face
U	upstream cell

Based on the above discussion, the two methods have complementary advantages and disadvantages. Sussman and Puckett [11] proposed a coupling method (coupled level-set and volume-of fluid method (CLSVOF)) taking advantages of both VOF and LS methods. In this method, the advection of the interface is fulfilled using the conservative VOF and the geometrical properties of the interface are calculated using the LS. A similar method was presented by Son and Hur [12]. In the method of van der Pijl et al. [13], there is no need to reconstruct the interface from the VOF in advecting the surface boundary. Yang et al. [14] developed an adaptive method such that unstructured triangular grids can be adopted. Ménard et al. [15] incorporated the ghost fluid method of Fedkiw et al. [16] into the CLSVOF such that the sharp discontinuity across the interface can be captured more accurately. In general, both the values of VOF and LS fields are obtained by solving their own advection equations. Sun and Tao [17] proposed a method in which the LS is determined from geometric consideration around the interface without solving the advection equation. In another method used by Albadawi et al. [18], the new LS is obtained by solving the equation used in the LS method for re-initialization.

An interface tracking procedure based on the VOF, termed conservative interpolation scheme for interface tracking (CISIT), had been developed by Tsui and Lin [19]. Unlike other VOF methods, the interface is simply characterized by the contour surface of VOF value 0.5. Comparing with the popular PLIC method, this method is easier to implement. In this study, a new CLSVOF method is proposed to combine the CIISIT and LS methods. The LS is initialized using the VOF. The signed distance property of the LS is then determined by solving the re-initialization equation.

Mathematical methods

The flow is assumed to be laminar and incompressible. The conservation equations for the two fluids can be given by one set of equations.

$$\nabla \cdot \vec{V} = 0 \tag{1}$$

$$\frac{\partial \rho \vec{V}}{\partial t} + \nabla \cdot (\rho \vec{V} \otimes \vec{V}) = -\nabla P + \nabla \cdot \tilde{\tilde{\tau}} + \rho \vec{g} + \vec{F}_\sigma \tag{2}$$

where $\tilde{\tilde{\tau}}$ represents the viscous stress and $\vec{F}_\sigma$ the surface tension force which is zero except in the cells containing the interface.

Within the frame of VOF methods, the interface is determined from the volume fraction α. It is either 0 or 1 in the single-phase cells and a value greater than 0 and less than 1 in the cells containing the interface. The transport equation for this function can be given as

$$\frac{\partial \alpha}{\partial t} + \nabla \cdot (\vec{V}\alpha) = 0 \tag{3}$$

Discretization of the differential equations is performed using a finite-volume scheme suitable for use of unstructured grids [20]. To solve the Navier–Stokes equations, the convection flux at cell faces is approximated using the van Leer scheme arranged in a flux limiter form while the diffusion flux by an over-relaxed scheme [21]. The coupling between momentum and continuity equations is tackled through an implicit treatment of the pressure gradients. Details of this approach can be found in the above references. The numerical methods related to the interface tracking and coupling of the VOF and LS methods are described in the following.

Numerical methods for interface tracking

In the interface tracking procedure of CISIT, the interface is simply represented by the contour surface of VOF value 0.5, which can easily be reconstructed. This procedure is briefly described in the following. More details can be found in reference [19].

To reconstruct the contour surface (contour line in 2-D problems), an interpolation practice is used (Figure 1). The original VOF values are stored at the centroid of grid cells. An interpolation practice is first performed to obtain the VOF on the grid nodes. The two end nodes of each side edge forming the cell are examined. The edge is intersected by the interface when the VOF of one node is less than 0.5 and the other greater than 0.5. The intersection points on the faces of the cell are connected. A continuous, piecewise linear interface can then be constructed after the same process proceeds throughout all the grid cells.

To illustrate the movement of the interface in a cell P, Figure 2 is prepared. The surface area wetted by a fluid on a face j of the cell is denoted by $\vec{s}_j^{\,w}$. The fluid flows into or out of the cell through this wetted area. The mass conservation of the fluid in this cell gives the following equation.

$$\frac{\Delta v}{\Delta t}(\alpha_P^n - \alpha_P^o) + \sum_j \vec{V}_j \cdot \vec{s}_j^{\,w} = 0, \tag{4}$$

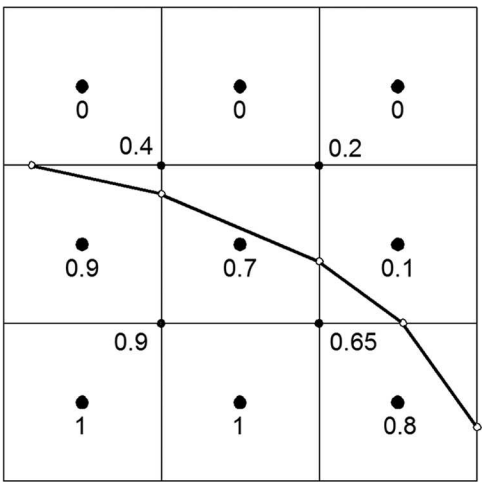

Figure 1. Illustration of the surface reconstruction.

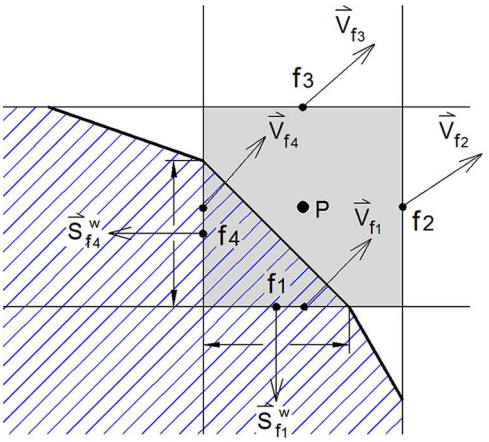

Figure 2. Illustration of the wetted area for an interface cell.

where $\vec{V}_j$ is the velocity vector on the jth face of the control surface. The sum is taken over all the faces. The equation leads to a new VOF value α_P^n for the interface cell.

The above calculation performs well, if the interface remains in the cell during time marching (Figure 3(*a*)). However, it cannot cope with the situation that the interface is moving out of the cell in the time interval. Four situations need to be considered: over filling ($\alpha_P^n > 1$), under filling ($\alpha_P^n < 1$), over depleting ($\alpha_P^n < 0$), and under depleting ($\alpha_P^n > 0$). Consider that a cell is filled with a fluid. When the fluid enters the cell, the value α_P^n will become greater than 1 (over filling) if the time interval Δt is large enough (Figure 3(*b*)). Similarly, the VOF will become less than 0 (over depleting) as the cell is over drained (Figure 3(*c*)). For the over-filling case, the excessive portion of the fluid ($\alpha_P^n - 1$) must be reallocated to the downstream cells such that the new VOF is equal to 1. For the over-depleting case, the over-drained part ($-\alpha_P^n$) must be retrieved from the downstream cells such that the new VOF equals to 0. These over-filling and over-depleting situations occur when the flow velocity is along the grid lines. As the flow is skew to the gridlines, α_P^n may remain to be less than 1 (under filling) when the interface is advancing to the neighboring cell. Similarly, α_P^n may be greater than 0 (under depleting) when the interface is retreating to the neighboring cell. For under filling, fluid ($1 - \alpha_P^n$) must be retrieved from the downstream cells to fill the cell such that the VOF value equals to 1. As for under depleting, the residual fluid in the cell (α_P^n) must be allocated to the downstream cells so that the VOF value becomes zero.

Coupling the VOF method with the LS method

The coupling takes advantage of the mass conservation of the VOF method and the interface smoothness of the LS method. The LS function ϕ is introduced as

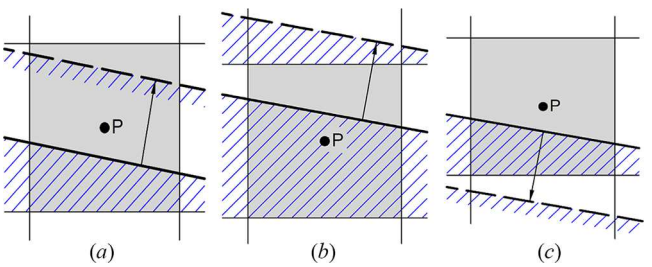

Figure 3. Illustration of the interface motion in a cell. (*a*) Normal filling, (*b*) over filling, and (*c*) over draining.

$$\phi(\vec{r},t)=\begin{cases} d(\vec{r}) & \vec{r} \text{ in the liquid phase} \\ 0 & \text{at the interface} \\ -d(\vec{r}) & \vec{r} \text{ in the gas phase} \end{cases} \tag{5}$$

where $d(\vec{r})$ is the shortest distance of the point $\vec{r}$ from the interface.

In LS methods or most CLSVOF methods, the advection equation for the level set function is solved first, followed by solving the re-initialization equation to recover the distancing property of the LS function. In the present method, this function is determined by solving the re-initialization equation only without needing to consider the advection equation, which simplifies the procedure significantly. This re-initialization equation is given by [2, 3]

$$\frac{\partial\phi}{\partial\tau}=S(\phi^0)(1-|\nabla\phi|) \tag{6}$$

Here τ is the fictitious time and ϕ^0 denotes the initial value of the LS function.

$$\phi^0(x)=\phi(x,0) \tag{7}$$

This initial value is given by the VOF function:

$$\phi^0(x)=(2\alpha-1)\Delta h \tag{8}$$

where Δh represents the grid size. As described above, the interface location is designated by the iso-contour $\alpha=0.5$ in the CISIT. Obviously, this initial distance function is zero at the interface, positive at the side $\alpha=1$, and negative on the other side $\alpha=0$. $S(\phi^0)$ in Eq. (6) is a sign function.

$$S(\phi^0)=\begin{cases} 1 & \text{if} \quad \phi^0>0 \\ 0 & \text{if} \quad \phi^0=0 \\ -1 & \text{if} \quad \phi^0<0 \end{cases} \tag{9}$$

For stability, the sign function is smoothed as

$$S(\phi^0)=\frac{\phi^0}{\sqrt{(\phi^0)^2+\Delta h^2}} \tag{10}$$

The solution of the equation converges when the condition $|\nabla\phi|=1$ is satisfied. The LS function is thus re-distanced from the interface.

The sharp changes in density and viscosity across the interface may cause instability in solving the Navier–Stokes equations. Therefore, these properties need to be diffused in the region of the interface.

$$\rho(\phi)=\rho_g(1-H(\phi))+\rho_l H(\phi) \tag{11}$$

$$\mu(\phi)=\mu_g(1-H(\phi))+\mu_l H(\phi) \tag{12}$$

Here $H(\phi)$ is the smoothed Heaviside function.

$$H(\phi)=\begin{cases} 0 & \text{if } \phi<-\varepsilon \\ 0.5\left[1+\frac{\phi}{\varepsilon}+\sin\left(\frac{\pi\phi}{\varepsilon}\right)\right] & \text{if } |\phi|\le\varepsilon \\ 1 & \text{if } \phi>\varepsilon \end{cases} \tag{13}$$

where ε denotes the transition region size for smoothing, being the order of the cell size.

The surface tension force is modeled by the CSF model of Brackbill et al. [10]. Since the LS is a continuous function, it helps in determining accurately the interface normal and curvature, as required in this model. This force can be calculated as

$$\vec{F}_\sigma = \sigma\kappa(\phi)\delta(\phi)\nabla\phi \tag{14}$$

where σ is the surface tension, and δ(ϕ) is the Dirac delta function used to limit the influence of the surface tension force to a narrow region around the interface.

$$\delta(\phi) = \begin{cases} \frac{1}{2\varepsilon}\left[1 + \pi\cos\left(\frac{\pi\phi}{\varepsilon}\right)\right] & \text{if} |\phi| \le \varepsilon \\ 0 & \text{otherwise.} \end{cases} \tag{15}$$

The curvature is calculated using the LS function.

$$\kappa(\phi) = \nabla\cdot\vec{n} = \nabla\cdot\left(\frac{\nabla\phi}{|\nabla\phi|}\right) \tag{16}$$

where $\vec{n}$ is the unit normal vector of the interface.

$$\vec{n} = \frac{\nabla\phi}{|\nabla\phi|} \tag{17}$$

Numerical methods for the re-initialization equation

The re-initialization equation can be rewritten into a hyperbolic form.

$$\frac{\partial\phi}{\partial\tau} + S\left(\phi^0\right)\vec{n}\cdot\nabla\phi = S\left(\phi^0\right) \tag{18}$$

in which $S\left(\phi^0\right)\vec{n}$ functions as the propagation velocity. An explicit scheme is used to find the new value ϕ^{n+1}.

$$\frac{\phi_P^{n+1} - \phi_P^n}{\Delta\tau} + S(\phi_P^0)|\nabla\phi_P| = S(\phi_P^0) \tag{19}$$

To satisfy the CFL condition, Δτ must be less than Δ*h*.

The gradient of ϕ is calculated using a finite-volume method suitable for use of unstructured grids.

$$\nabla\phi_P = \frac{1}{\Delta v}\sum_f \phi_f\vec{s}_f \tag{20}$$

where the subscript *f* denotes the face value, $\vec{s}_f$ is the surface vector of a cell face, and the sum is over all the faces of the considered *P*-cell. Due to the hyperbolic characteristics, the face value is approximated using the upwind scheme, depending on the sign of $S\left(\phi^0\right)\vec{n}$.

$$\phi_f = \begin{cases} \phi_P & \text{if } \phi_{Ci} - \phi_P > 0 \text{ and } \phi_P^0 > 0 \\ \phi_{Ci} & \text{if } \phi_{Ci} - \phi_P < 0 \text{ and } \phi_P^0 > 0 \\ \phi_P & \text{if } \phi_{Ci} - \phi_P < 0 \text{ and } \phi_P^0 < 0 \\ \phi_{Ci} & \text{if } \phi_{Ci} - \phi_P > 0 \text{ and } \phi_P^0 < 0 \end{cases} \tag{21}$$

where ϕ_{Ci} is the value on the neighboring cell centroid (Figure 4).

The above method is first-order accurate only. Its accuracy can be improved by the following procedure. After the gradient is calculated using the first-order upwind scheme, a new face value can be obtained by

$$\phi_f = \phi^U + \nabla\phi^U\cdot\vec{\delta}_{U-f} \tag{22}$$

where ϕ^U and $\nabla\phi^U$ are the value of ϕ and its gradient at the upwind cell *U* obtained from Eq. (20), and $\vec{\delta}_{U-f}$ is the distance vector directed from the upwind cell centroid *U* to the face *f* (Figure 5). A

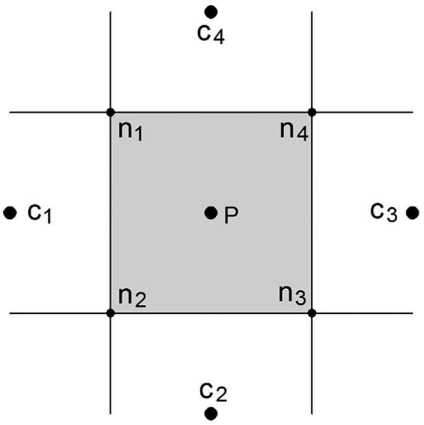

Figure 4. Illustration of neighboring cells and cell nodes.

problem is raised using this second-order scheme because overshoots or undershoots may appear. To overcome this, a limiter γ is assigned to the gradient part such that the face value is bounded.

$$\phi_f = \phi^U + \gamma \nabla \phi^U \cdot \vec{\delta}_{U-f} \tag{23}$$

To determine the limiter, a method similar to that of Barth and Jespersen [22] is used. The idea is to restrict the linearly reconstructed function in the range between the maximum and minimum of neighboring cell values. First, compute maximum and minimum values as

$$\phi^{max} = \max(\phi_P, \phi_{Ci}) \tag{24}$$

$$\phi^{min} = \min(\phi_P, \phi_{Ci}) \tag{25}$$

Note that the subscript P here denotes the cell upwind of the considered face and the subscript Ci denotes all the cells neighboring to this upwind cell. For linear reconstruction, extrema of ϕ in the cell occur at the vertices. The nodal value ϕ_{ni} on each vertex (Figure 4) can be obtained by interpolation from surrounding centroid values. The limiter for each vertex node γ_{ni} is determined by

$$\gamma_{ni} = \begin{cases} 1 & \text{if } \phi_{ni} = \phi_P \\ \min\left(1, \frac{\phi^{max} - \phi_P}{\phi_{ni} - \phi_P}\right) & \text{if } \phi_{ni} - \phi_P > 0 \\ \min\left(1, \frac{\phi^{min} - \phi_P}{\phi_{ni} - \phi_P}\right) & \text{if } \phi_{ni} - \phi_P < 0 \end{cases} \tag{26}$$

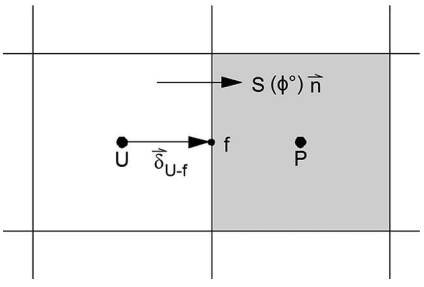

Figure 5. Illustration of the upwind cell.

Finally, the limiter is given by

$$\gamma = \min(\gamma_{ni}) \tag{27}$$

After all new face values are obtained, they are substituted into Eq. (20) to recalculate the gradient.

It was pointed out by Russo and Smereka [23] that the position of the interface may move in the interface cell during iteration. This movement is due to that in the discretization across the interface, the upwind property is violated; i.e., information on the other side of the interface is used in calculation of the gradient. To overcome this difficulty, the gradient in the cells containing the interface is calculated in the following way. The ratio of $\nabla\phi$ and its initial value $\nabla\phi^o$ in the interface cell can be approximated by

$$\frac{\nabla\phi}{\nabla\phi^0} = \frac{\phi_P - \phi_{interface}}{\phi_P^0 - \phi_{interface}^0} \tag{28}$$

Since both $\phi_{interface}$ and $\phi^0_{interface}$ are zero, the gradient of ϕ can be calculated as

$$\nabla\phi = \nabla\phi^0 \frac{\phi_P}{\phi_P^0} \tag{29}$$

Results and discussion

The solution method to solve the re-initialization equation for the LS is verified first. The CLSVOF method is then tested on a bubble at equilibrium to examine the spurious currents generated due to the surface tension model. It is followed by considering the rising of a bubble in quiescent water.

Verification of the method for the LS calculation

The numerical method used to solve for the LS is verified by considering a variety of interface geometries. Figure 6 shows the LS distribution for a circle calculated by the second-order scheme and the bounded second-order scheme. The computational grid contains 20 × 20 cells. It is obvious that the distance function is not smooth inside the circle obtained by the former because of the overshoot/undershoot problem. This problem also leads to nonconvergence of the solution iteration. The results for three different shapes (a square, a diamond, and a circle with a square cut) calculated by the bounded scheme on a 40 × 40 grid are shown in Figure 7. The contour lines show accurate signed distances from the interface regardless of the interface geometry.

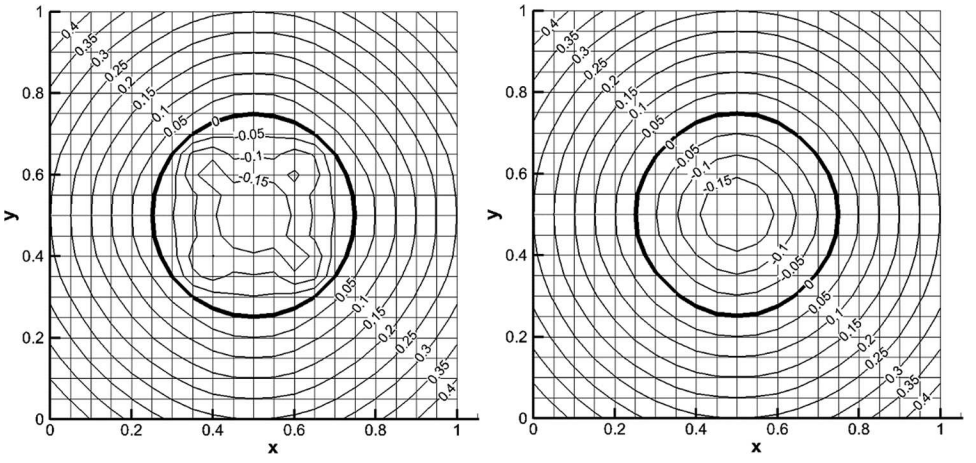

Figure 6. Distribution of the LS function calculated by (*a*) second-order scheme and (*b*) bounded second-order scheme.

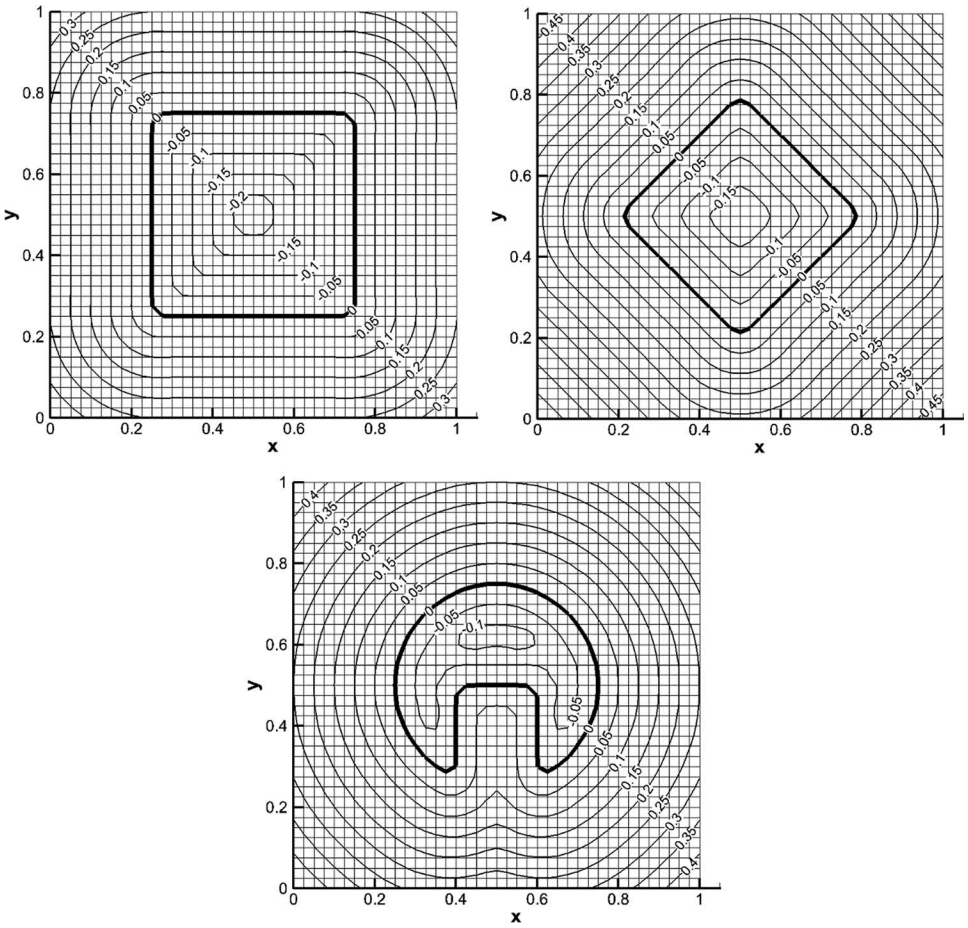

Figure 7. Distribution of the LS function for different interface geometries.

Tests on spurious currents

Spurious currents were observed in studies [18, 24, 25] when the CSF model is used for calculating the surface tension force. They are regarded as numerical errors which should be minimized. To assess our method, a circular bubble under no effect of gravity is considered. The physical properties for the gas phase are $\rho_g = 1\ \mathrm{kg/m^3}$, $\mu_g = 10^{-5}\ \mathrm{kg/}ms$, and those for the liquid phase are $\rho_l = 1,000\ \mathrm{kg/m^3}$, $\mu_l = 0.001\ \mathrm{kg/}ms$. The surface tension is $\sigma = 0.01\ \mathrm{kg/s^2}$. The diameter of the bubble is $d = 0.01$ m. The bubble is placed at the center of a square region of size 0.05 m. Calculations are undertaken on a 100×100 grid for 0.1 s.

Figure 8 shows the velocity vectors obtained by the CLSVOF and the CISIT. A number of spurious vortex flows are clearly identified within the bubble. The strength of the vortices is much weaker in the calculations using the CLSVOF. Quantitative comparison of the two methods is shown in Table 1. The error in the magnitude of the spurious current is given by the maximum velocity norm l_∞^V. The error in the interface curvature is calculated by the following l_2 norm.

$$l_2^C = \sqrt{\frac{\sum_{i=1}^{N} (\kappa R - \kappa_{\mathrm{exact}} R)^2}{N}} \tag{30}$$

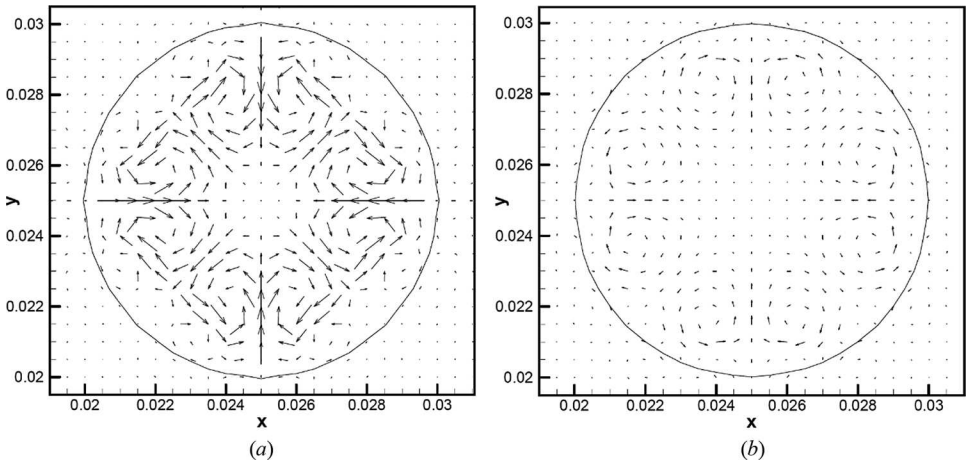

Figure 8. Velocity vectors calculated by (*a*) CISIT and (*b*) CLSVOF.

Table 1. Error norms in velocity, curvature, and pressure.

	l_∞^V (m/s)	l_2^C	E^P (%)
CISIT	0.1034	0.4714	0.144
CLSVOF	0.0326	0.0894	0.052

where N is the number of the interface cells. The exact curvature of the bubble is equal to $2/d$. Therefore, the theoretical pressure difference between the inside region and outside region of the bubble is $2\sigma/d$. The error in the pressure is calculated by

$$E^P = \frac{|\Delta P - \Delta P_{\text{exact}}|}{\Delta P_{\text{exact}}} \tag{31}$$

where ΔP is the difference between the averaged pressures inside and outside the bubble. It can be seen from the table that the reduction of the error in velocity, curvature, and pressure is significant when the CLSVOF method is adopted in calculations.

Single rising bubble

The initial diameter of the bubble is $d = 0.01$ m and the water tank is in the size $5d \times 5d \times 5d$. Only a quarter of the domain is considered in calculations. Symmetrical condition is assumed on the side boundaries, and the top boundary is open.

Three flow cases are under investigation: (Eo = 1, Mo = 10^{-3}), (Eo = 10, Mo = 1), and (Eo = 100, Mo = 10^3), where Eo = $\Delta\rho g d^2/\sigma$ is the Eovots number and Mo = $g\mu_l^4/\rho_l\sigma^3$ the Morton number. As can be found from the Grace diagram [26], the first case is located in the spherical regime, the second case falls on the edge between the spherical and ellipsoidal regimes, and the last case on the margin of the dimpled cap regime. Figures 9 and 10 show the bubble shapes at the terminal velocity predicted by the VOF-based CISIT method and the CLSVOF method using two grids containing $25 \times 25 \times 150$ and $50 \times 50 \times 300$ cells. In general, the bubble shapes are in accordance with those indicated in the Grace diagram. The large surface tension of the first case keeps the bubble round. As the surface tension decreases, the geometry deviate from the round shape. The results obtained by the two methods are alike except for the last case. The bubble has a cap shape with a dimple at the lower surface when the fine grid is used in computations. Comparing with the CISIT, the depth of the dimple is lower by the CLSVOF. With the low-resolution grid, the bubble predicted by the CLSVOF remains

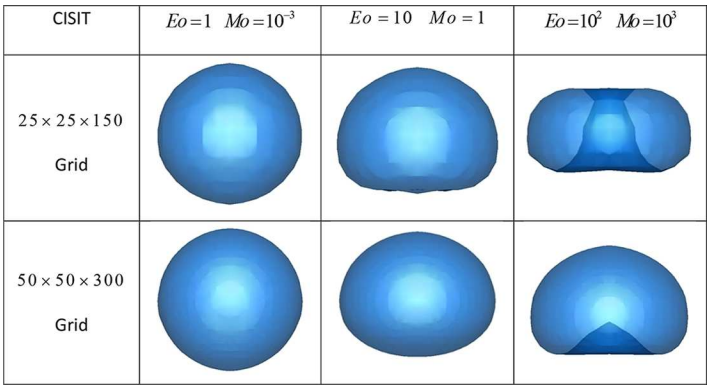

Figure 9. Bubble shape at terminal velocity calculated by CISIT.

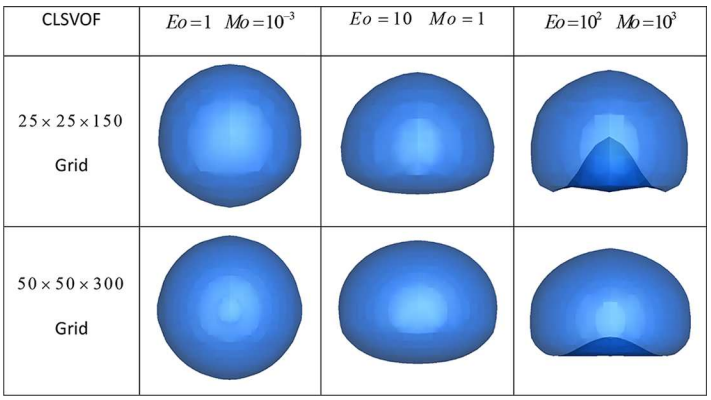

Figure 10. Bubble shape at terminal velocity calculated by CLSVOF.

Table 2. Reynolds numbers at terminal velocity for rising bubble.

CISIT	Re = 4.04	Re = 3.42	Re = 3.15
CLSVOF	Re = 3.15	Re = 3.35	Re = 3.03

as the cap shape whereas by the CISIT, the dimple penetrates through the bubble to form a toroidal shape. The cause of the differences is attributed to the surface tension force which can be calculated more accurately by the CLSVOF.

The resulting Reynolds numbers ($Re = \rho_l U d/\mu_l$, based on the terminal velocity U of the rising) are listed in Table 2. The Reynolds numbers for the three cases are about a value of 2 according to the Grace diagram. It can be detected that the Reynolds numbers computed by the CLSVOF have smaller scatter and their values are closer to the Grace's correlation.

Conclusion

A new method coupling the VOF-based CISIT method and the LS method was proposed. In this method, the LS function is obtained by solving the re-initialization equation directly without needing to consider the advection equation for the LS. A high-resolution bounded scheme within the frame of finite-volume methods was used to solve the re-initialization equation. Accurate signed distances

were obtained for a variety of interface shapes. The spurious current in a circular bubble at equilibrium, generated due to the surface tension model, was examined. It was seen that with use of the CLSVOF, the strength of the spurious flow is much lower and the calculation of the curvature is more accurate in comparison with the CISIT. In simulating the rising of a bubble, the characteristics of the bubble at terminal velocity are closer to the experimental correlation by the coupling method than by the VOF method.

Acknowledgments

This work was supported by the Ministry of Science and Technology, Republic of China, under the Contract Number MOST 104-2221-E009-152.

References

[1] S. Osher and J. A. Sethian, Fronts Propagating with Curvature-Dependent Speed: Algorithms Based on Hamilton-Jacobi Formulations, *J. Comput. Phys.*, vol. 79, pp. 12–49, 1988.
[2] M. Sussman, P. Smereka, and S. Osher, A Level Set Approach for Computing Solutions to Incompressible Two-Phase Flow, *J. Comput. Phys.*, vol. 114, pp. 146–159, 1994.
[3] M. Sussman, E. Fatami, P. Smereka, and S. Osher, An Improved Level Set Method for Incompressible Two-Phase Flows, *Comput. Fluids*, vol. 27, pp. 663–680, 1998.
[4] J. Lee and G. Son, A Level-Set Method for Analysis of Particle Motion in an Evaporating Microdroplet, *Numer. Heat Transfer B*, vol. 67, pp. 25–46, 2015.
[5] C. W. Hirt and H. D. Nichols, Volume of Fluid (VOF) Method for the Dynamics of Free Boundaries, *J. Comput. Phys.*, vol. 39, pp. 201–225, 1981.
[6] D. L. Youngs, Time-Dependent Multi-Material Flow with Large Fluid Distortion, in K. W. Morton and M. J. Baines (eds.), *Numerical Methods for Fluid Dynamics*, vol. 24, pp. 273–285, Academic Press, New York, 1982.
[7] W. J. Rider and D. B. Kothe, Reconstructing Volume Tracking, *J. Comput. Phys.*, vol. 141, pp. 112–152, 1998.
[8] J. E. Pilliod Jr. and E. G. Puckett, Second-Order Accurate Volume-of-Fluid Algorithms for Tracking Material Interfaces, *J. Comput. Phys.*, vol. 199, pp. 465–502, 2004.
[9] M. Huang, L. Wu, and B. Chen, A Piecewise Linear Interface-Capturing Volume-of-Fluid Method Based on Unstructured Grids, *Numer. Heat Transfer B*, vol. 61, pp. 412–437, 2012.
[10] J. U. Brackbill, D. B. Kothe, and C. Zemach, A Continuum Method for Modeling Surface Tension, *J. Comput. Phys.*, vol. 100, pp. 335–354, 1992.
[11] M. Sussman and E. G. Puckett, A Coupled Level Set and Volume-of-Fluid Method for Computing 3D and Axisymmetric Incompressible Two-Phase Flows, *J. Comput. Phys.*, vol. 162, pp. 301–337, 2000.
[12] G. Son and N. Hur, A Coupled Level Set and Volume-of-Fluid Method for the Buoyancy-Driven Motion of Fluid Particles, *Numer. Heat Transfer B*, vol. 42, pp. 523–542, 2002.
[13] S. P. van der Pijl, A. Segal, C. Vuik, and P. Wesseling, A Mass-Conserving Level-Set Method for Modeling of Multi-Phase Flows, *Int. J. Numer. Methods Fluids*, vol. 47, pp. 339–361, 2005.
[14] X. F. Yang, A. J. James, J. Lowengrub, X. M. Zheng, and V. Cristini, An Adaptive Coupled Level-Set/Volume-of-Fluid Interface Capturing Method for Unstructured Triangular Grids, *J. Comput. Phys.*, vol. 217, pp. 364–394, 2006.
[15] T. Ménard, S. Tanguy, and A. Berlemont, Coupling Level Set/Vof/Ghost Fluid Methods: Validation and Application to 3D Simulation of the Primary Break-Up of a Liquid Jet, *Int. J. Multiphase Flow*, vol. 33, pp. 510–524, 2007.
[16] R. P. Fedkiw, T. Aslam, B. Merriman, and S. Osher, A Non-Oscillatory Eulerian Approach to Interfaces in Multimaterial Flows (the Ghost Fluid Method), *J. Comput. Phys.*, vol. 152, pp. 457–492, 1999.
[17] D. L. Sun and W. Q. Tao, A Coupled Volume-of-Fluid and Level Set (VOSET) Method for Computing Incompressible Two-Phase Flows, *Int. J. Heat Mass Transfer*, vol. 53, pp. 645–655, 2010.
[18] A. Albadawi, D. B. Donoghue, A. J. Robinson, D. B. Murray, and Y. M. C. Delaure, Influence of Surface Tension Implementation in Volume of Fluid and Coupled Volume of Fluid with Level Set Methods for Bubble Growth and Detachment, *Int. J. Multiphase Flow*, vol. 53, pp. 11–28, 2013.
[19] Y.-Y. Tsui and S.-W. Lin, A VOF-Based Conservative Interpolation Scheme for Interface Tracking (CISIT) of Two-Fluid Flows, *Numer. Heat Transfer B*, vol. 63, pp. 263–283, 2013.
[20] Y.-Y. Tsui and Y.-F. Pan, A Pressure-Correction Method for Incompressible Flows Using Unstructured Meshes, *Numer. Heat Transfer B*, vol. 49, pp. 43–65, 2006.
[21] Y.-Y. Tsui and T.-C. Wu, A Pressure-Based Unstructured-Grid Algorithm Using High Resolution Schemes for All-Speed Flows, *Numer. Heat Transfer B*, vol. 53, pp. 75–96, 2008.

[22] T. J. Barth and D. C. Jespersen, The Design and Application of Upwind Schemes on Unstructured Meshes, AIAA 89–0366, *27th Aerospace Sciences Meeting*, Reno, NV, 1989.
[23] G. Russo and P. Smereka, A Remark on Computing Distance Functions, *J. Comput. Phys*, vol. 163, pp. 51–67, 2000.
[24] B. Lafaurie, C. Nardone, R. Scardovelli, S. Zaleski, and G. Zanetti, Modelling Merging and Fragmentation in Multiphase Flows with SURFER, *J. Comput. Phys.*, vol. 113, pp. 134–147, 1994.
[25] Y. Renardy and M. Renardy, PROST: A Parabolic Reconstruction of Surface Tension for the Volume-of-Fluid Method, *J. Comput. Phys.*, vol. 183, pp. 400–421, 2002.
[26] J. R. Grace, Shape and Velocities of Bubbles Rising in Infinite Liquids, *Trans. Inst. Chem. Eng.*, vol. 51, pp. 116–120, 1973.